Front. Earth Sci. 2021, 15(4): 737–753
https://doi.org/10.1007/s11707-021-0893-x

RESEARCH ARTICLE

Paleoenvironment controls on organic matter accumulation in transitional shales from the eastern Ordos Basin, China

Jianwei LV[1,2], Songhang ZHANG (✉)[1], Ning YANG (✉)[3], Chunbo FU[4], Xinlu YAN[1], Yang LI[1]

1 School of Energy Resources, China University of Geosciences, Beijing 100083, China
2 Chinese Academy of Natural Resources Economics, Beijing 101149, China
3 Huadian Coal Industry Group Co., Ltd., Beijing 100035, China
4 Second Oil Production Plant, PetroChina Changqing Oilfield Company, Qingyang 745100, China

Abstract To investigate the paleoenvironmental controls on organic matter accumulation of Upper Paleozoic shales in the eastern Ordos Basin, China, 26 shale samples were collected from two wells drilled into the Shanxi and Taiyuan Formations. The total organic carbon (TOC) content, mineral compositions and elemental geochemistry of the samples were analyzed. Quartz (35.42%) and clay minerals (48.34%) are the dominant minerals and trace elements (Li, Cs, Cu, V, Co, and Cr) are commonly enriched in the shale samples compared to the Upper Continental Crust. C-values (ranging from 0.2 to 4.5), chemical indices of weathering (CIW) values (48.82 to 99.11), and Sr/Cu ratios (1.00 to 11.05) suggest that the paleoclimate was humid in the study area during the Late Paleozoic. Elemental redox indices (e.g., $Al_2O_3/(Al_2O_3+Fe_2O_3)$, V/Cr, Ni/Co, V/(V + Ni) and U/Th) indicate a dysoxic to oxic paleoenvironment characterized by transitional sedimentary deposits in a continental margin setting. In addition, chemical index of alteration (CIA, ranging from 77.92% to 98.36%) and CIW (89.19% to 99.11%) values suggest that there was intense chemical weathering in the study area, while the Al_2O_3-CaO^* + Na_2O-K_2O (A-CN-K) ternary diagram demonstrates that the shales were not subjected to potassium metasomatism during diagenesis. Al_2O_3/TiO_2 and TiO_2/Zr ratios, as well as REE characteristics suggest a felsic source rocks and discount seawater as an REE source. Ce anomalies indicate an oxic environment with terrigenous input during black shale deposition, and LREE enrichment with negative Eu anomalies suggests that both shale formations were affected by detrital input rather than hydrothermal fluids. The correlation of TOC (ranging from 1.10% to 6.39%, with an average of 2.77%) with trace elemental redox indices (Sr/Cu, Sr/Ba, V/Cr, and U/Th) indicates that a warm-humid, dysoxic to oxic environment preserved much of the organic matter.

Keywords Late Paleozoic, shale, geochemistry, paleoenvironment, eastern Ordos Basin

1 Introduction

With increasing global demand for energy, shale gas has received increasing attention and the remarkable success of shale gas production in the United States has stimulated shale gas exploration worldwide (Bezard et al., 2011; Chermak and Schreiber, 2014; Newport et al., 2016; Han et al., 2018; Li et al., 2019a). China has encouraged the development of shale gas, and marine shales from the Lower Silurian Longmaxi and Lower Cambrian Niutitang formations are the key targets (Wang et al., 2012; Wang et al., 2015; Gao et al., 2016). A number of studies have focused on pore structure, geochemical characteristics, and paleoenvironment of South China shale (Kasanzu et al., 2008; Hu et al., 2016; Wang et al., 2016; Zhang et al., 2016), while the transitional and terrestrial shale formations in North China have also garnered some attention (Michard and Albarède, 1986; Fu et al., 2011a; Tribovillard et al., 2006). Most studies of terrestrial shale have focused on reservoir quality and organic geochemistry (Algeo and Maynard, 2004; Yang et al., 2008). The chemical composition of shale provides important information about paleoenvironmental conditions and paleotectonic setting, while the geochemical behavior of major and trace elements can reveal information about the paleoclimate during shale deposition. Trace elements are

Received August 7, 2020; accepted March 3, 2021

E-mails: zl062051@163.com (Songhang ZHANG)
yncugb@163.com (Ning YANG)

thought to reflect specific depositional environments and paleoclimates (Hofmann et al., 2016; Vosoughi Moradi et al., 2016a, 2016b). In recent years, element geochemistry has been widely applied to analyze the origins of sedimentary rocks (Stepanova et al., 2015; Udchachon et al., 2017). In addition, because the paleoenvironment appears to play an important role in the development of shale porosity (Li et al., 2016; Bai et al., 2017), there may be a relationship between trace element compositions and porosity.

The Ordos Basin, a large carton basin in China, has numerous fossil fuel deposits that have attracted considerable attention (Xiao et al., 2005; Yang et al., 2008). Coal-bearing deposits in the basin consist of Pennsylvanian, Permian, Triassic, and Jurassic strata, including coal beds, tight sandstone and coal-bearing shale. The petrology and stratigraphy of Late Paleozoic shale in the Ordos Basin have been subject of numerous studies, and much attention has been paid to coal (Yang et al., 2015; Sun et al., 2016), coalbed methane (CBM) (Zhang et al., 2010; Xu et al., 2015; Li et al., 2020a, 2020b; Zhao et al., 2016a), and shale deposited as terrestrial facies of this region (Xu et al., 2012; Qiu et al., 2014, 2015). However, there has been less focus on transitional shale in the Ordos Basin and its elemental geochemical characteristics.

This study aims to provide new insights for future development of transitional shale based on an integrated elemental geochemical study of Late Paleozoic shale in the eastern Ordos Basin. We utilized scanning electron microscopy (SEM), X-ray diffraction (XRD), X-ray fluorescence (XRF), and inductively coupled plasma mass spectrometry (ICP-MS), to determine the geochemical characteristics of transitional shale. We describe the paleoclimate and paleoenvironment in the study area during the Late Paleozoic and investigate their relationships with total organic carbon (TOC) and trace element indicators in shales, which provide an important basis for future research on Late Paleozoic shale gas potential. Furthermore, this study provides valuable insights for a comprehensive evaluation of transitional shale.

2 Geological setting

The Ordos Basin is the second-largest sedimentary basin in China, located to the west of the North China Platform (Dai et al., 2006; Yang et al., 2008). It covers an area of 25×10^4 km^2 and contains sediments with a total thickness of 4000–6000 m. The basement tectonic configuration is used to divide the basin into six major subdivisions: the Yimeng Uplift, the Weibei Uplift, the Jinxi Fold Belt, the Shanbei Slope, the Tianhuan Depression and the Western Edge Thrust Belt (Fig. 1). The structural framework of the basin is a very large asymmetric syncline with a gentle slope of 0.5°–1.0° toward the east and north, and a slightly steeper slope of 2°–3° toward the west and south. The structure of the basin is simple; large faults occur at the western edges of the basin, separating the Western Edge Thrust Belt from the Tianhuan Depression. With the exception of a few small-scale paleofaults, no major faults have been found within the basin (Xiao et al., 2005). The eastern margin of the Ordos Basin is a large westward-sloping monocline with a slope of 3°–10° characterized by relatively simple and stable structures. There are some slight northeast and north–northeast trending folds as well as a few small-scale faults (Zhao et al., 2016b).

Late Paleozoic (Taiyuan and Shanxi Formations) organic-rich shale is widely distributed in the Jinxi Fold Belt, along the eastern margin of the Ordos Basin. Wells number XY1 and LY4 are located in Xixian County and Liulin County, respectively, within the Jinxi Fold Belt (Fig. 1). The Shanxi and the Taiyuan Formations around well LY4 range in depth from 1371.0 m to 1487.0 m, while depths at well XY1 range from 1431.0 m to 1550.0 m (Fig. 2). Lithologically, the Shanxi and Taiyuan Formations are composed of coal, shale (clay, sandy and silty shale), sandstone, and limestone (Fig. 2).

3 Sampling and methods

A total of 14 samples from well XY1 and 12 samples from well LY2 were analyzed for total organic carbon (TOC), mineral composition, and major and trace elements (including rare earth elements (REEs)). All black shale samples were sealed in polyethylene bags to prevent oxidation. A portion of each sample was ground to pass through a 200 mesh sieve, and stored in brown glass bottles for chemical analysis.

Total organic carbon was determined at the Beijing Research Institute of Uranium Geology, using a chemical method according to the Chinese National Standard GB/T19145-2003. Mineral composition was determined using powder X-ray diffraction spectrometry (XRD). The XRD measurements were carried out with a Panalytical X' Pert PRO MPD equipped with a Cu-target tube and a curved graphite monochromator, operating at 40 kV and 40 mA. Samples were step-scanned from 5° to 70° with a step size of 0.02° (2θ). These procedures followed the method described by Chinese Oil and Gas Industry Standards SY/T 6201-2010 and SY/T 5163-2010.

Major elements were analyzed using an X-ray fluorescence spectrometer (AB-104L), with better than 0.01% analytical precision. For trace elements, the powdered samples were first leached with 2 N HCl to remove carbonate and calcium phosphate minerals. Next, 75 mg of powder were dissolved in 6 mL of 6 N HF/6 N HNO_3 (1:2) at about 180°C for 12–24 h, and dried. Dry samples were diluted with HNO_3 and further diluted with ultrapure H_2O to a volume of 100 mL. These solutions were analyzed using inductively coupled plasma mass spectrometry (ICP-MS) (ELAN DRC-e). Analytical precision and accuracy

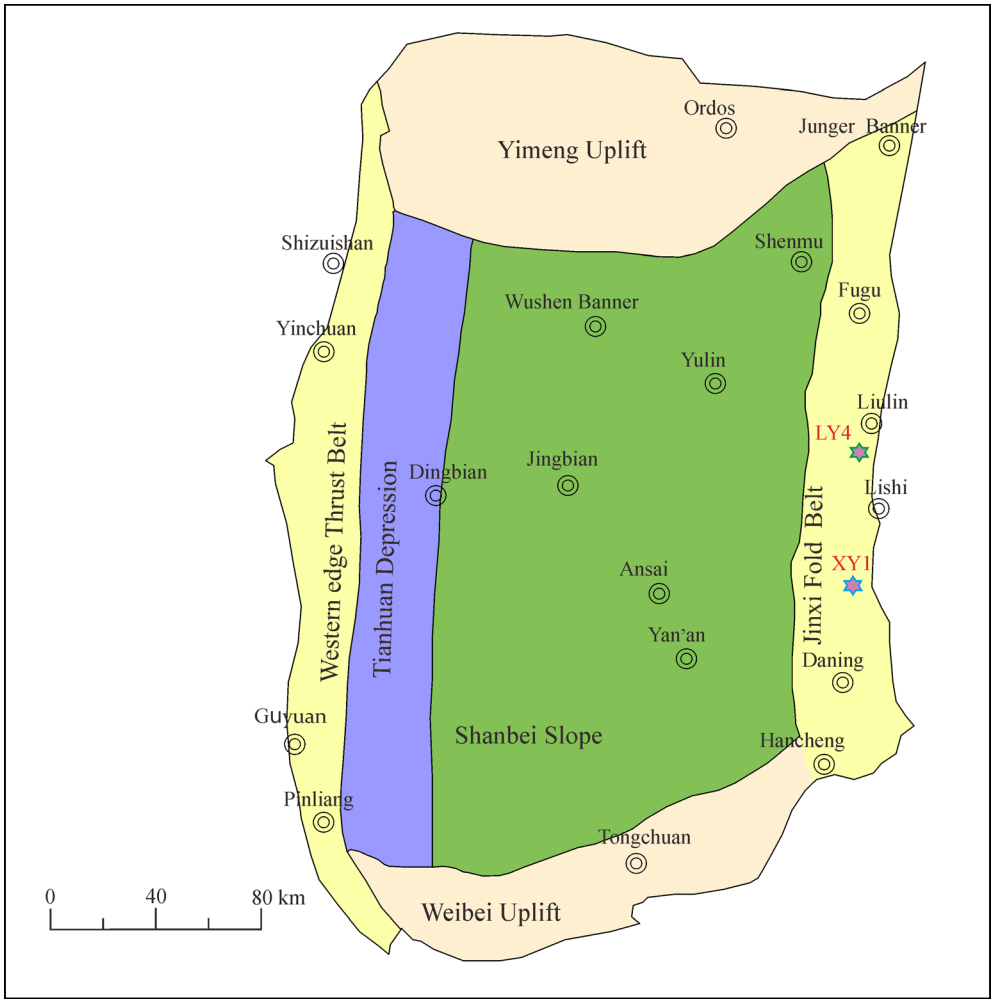

Fig. 1 Simplified geological map of the Ordos Basin. Wells XY1 and LY4 in the study area are shown.

were evaluated by duplicate analyses of samples and two international standard reference samples, BHVO-1 and AGV-1. Analytical precision for trace element concentrations is better than 5% (Zhang et al., 2016). All chemical analyses were conducted at the CNNC Beijing Research Institute of Uranium Geology, China.

4 Results

4.1 TOC content and thermal maturity

For well LY4, TOC for samples from the Shanxi Formation (LY401-LY405) ranges from 1.10% to 6.39%, with an average of 3.03%. For samples from the Taiyuan Formation (LY406-LY412), TOC varies between 1.10% and 3.82%, with an average of 2.16%. At well XY1, TOC for samples from the Shanxi Formation (XY101-XY106) ranges from 1.51% to 4.65%, with an average of 2.75%. For samples from the Taiyuan Formation (XY107-XY114), TOC varies between 2.25% and 4.15% with an average of 3.16%. The shale samples are enriched in TOC and their vitrinite reflectance (R_o) values range from 1.87% to 3.65% with an average of 2.85%, indicating an over-mature thermal maturity of organic matter.

4.2 Mineral compositions

Mineral phase percentages were calculated based on X-ray diffraction spectrometry (XRD) results which show that minerals in shale samples from the eastern margin of the Ordos Basin consist of quartz (average of 35.4%), clay minerals (48.3%), calcite (11.3%), siderite (5.7%), pyrite (4.9%), ankerite (4.0%) and feldspar (3.3%) (Fig. 3).

Quartz is a common mineral in shale (Fu et al., 2011b; Chermak and Schreiber, 2014). In samples from the Ordos Basin, quartz content ranges from 9.9% to 51.2%, with an average of 35.4%. Most samples have quartz contents between 30% and 50%. Compared to the Lower Silurian Longmaxi shale from South China (with an average quartz

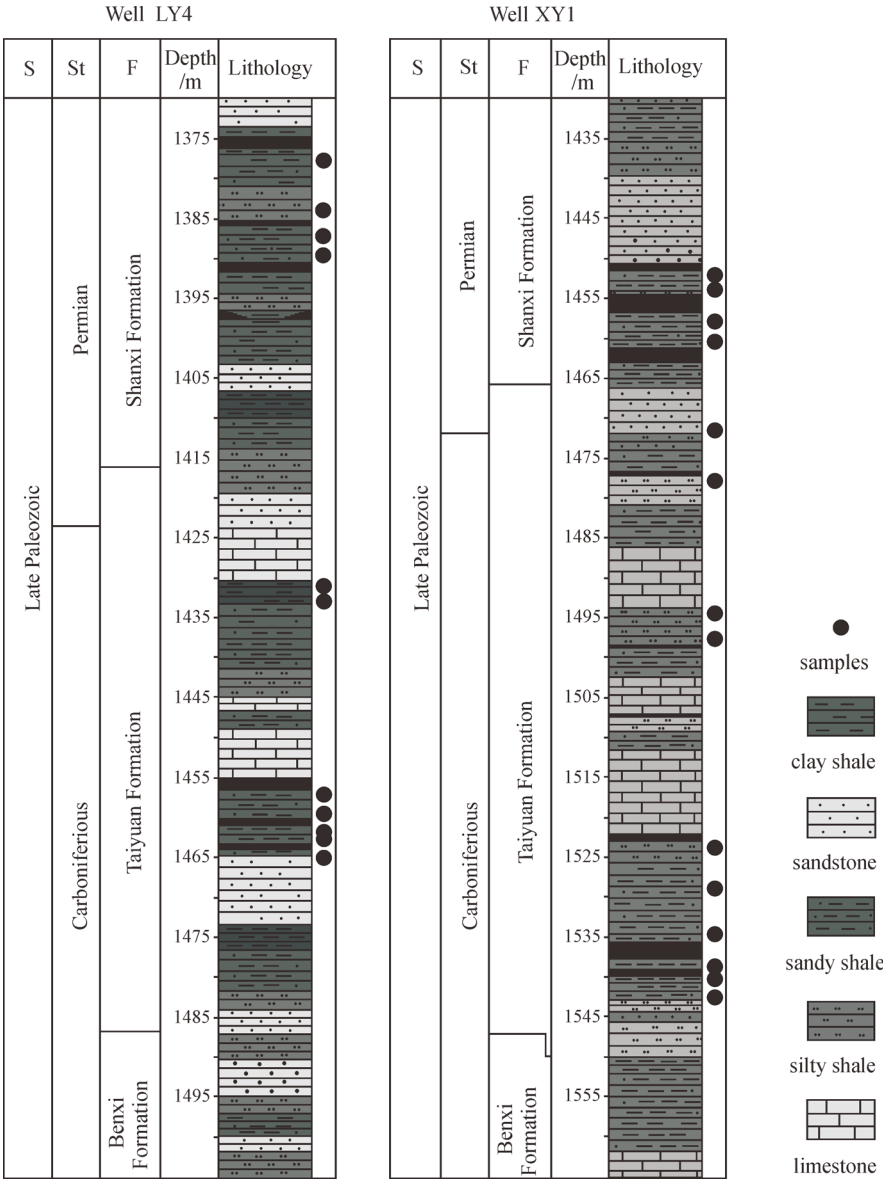

Fig. 2 Stratigraphic columns for wells XY1 and Well LY4.

content of 53.3%) (Hu et al., 2016), Carboniferous and Permian shales from North China are relatively low in quartz.

Another dominant mineral in shale is clay (Chermak and Schreiber, 2014; He et al., 2016). Clay minerals were identified using scanning electron microscopy (SEM) (Fig. 3(a)). Clay content varies between 11.3% and 81.3% (average of 48.3%), with most samples ranging from 40% to 60%. Clay minerals consist of kaolinite (average of 38.2%), illite (14.7%) (Fig. 3(b)), illite-smectite mixed layer minerals (39.9%), and chlorite (9.1%).

Carbonate minerals, including calcite, siderite, and ankerite, were also detected in the Late Paleozoic shales. Calcite was detected in most of the Taiyuan Formation samples and in a few samples from the Shanxi Formation, varying in content from 0.6% to 5.8%, except for samples LY408 (30.6%) and XY107 (69.8%). Pyrite is present in most samples at concentrations up to 10.3%, occurring mainly as fine particles (Fig. 3(c)) and framboidal pyrite (Fig. 3(d)). Feldspar concentrations range from 1.3% to 6.2%, with plagioclase content (average of 2.4%) higher than that of K-feldspar (1.7%).

Shale samples from different formations show differences in mineral composition (Fig. 4). Samples from the Shanxi Formation contain fewer carbonate minerals than those from the Taiyuan Formation, while clay mineral concentrations in shale samples from the Shanxi Formation are higher than in samples from the Taiyuan Formation.

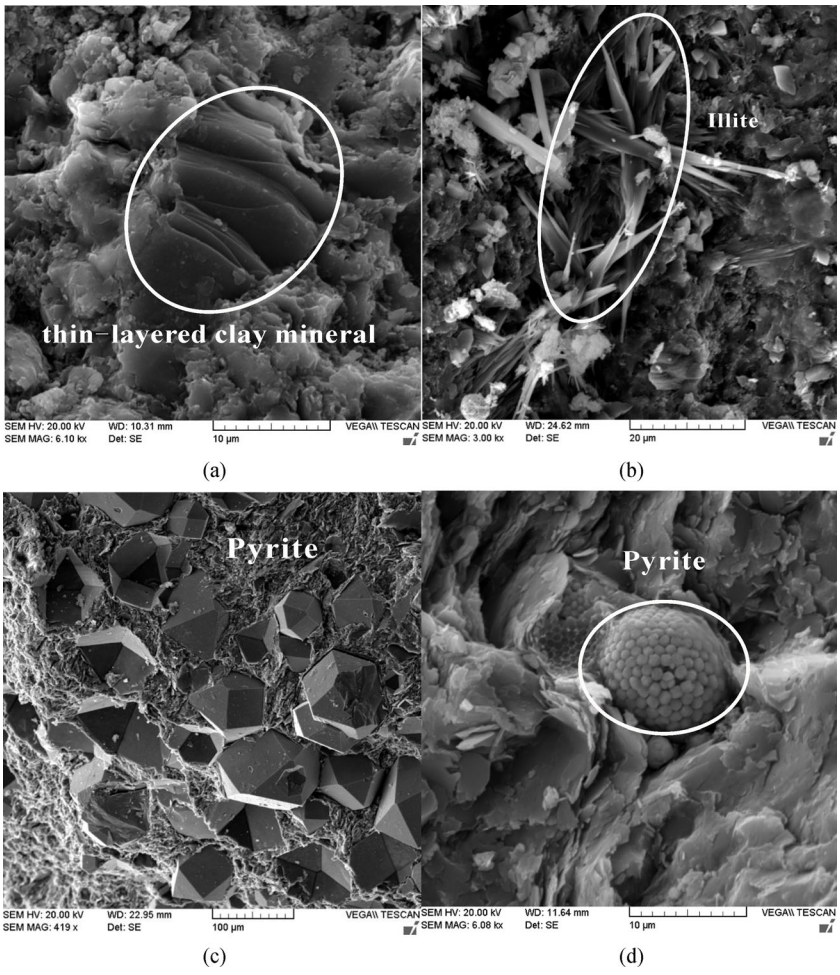

Fig. 3 SEM photomicrographs showing mineral characteristics of the shales ((a) clay minerals; (b) illite; (c) and (d) pyrite).

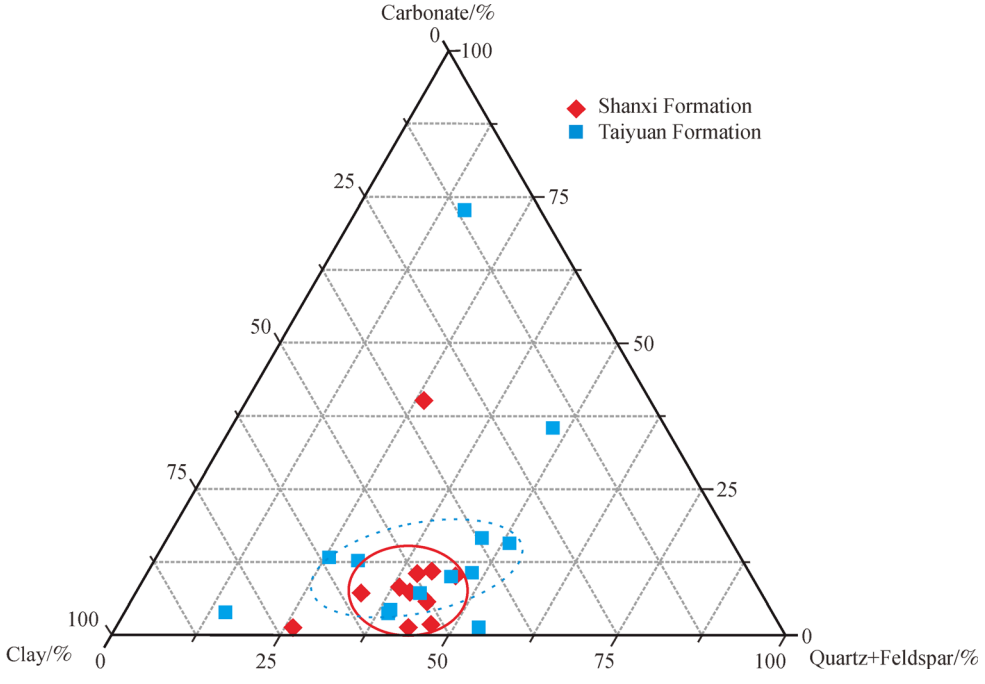

Fig. 4 Mineral characteristics of samples from Shanxi and Taiyuan Formations.

4.3 Major and trace elements

4.3.1 Major elements

The results for major element analyses are listed in Table 1. Major elements in Late Paleozoic shales are dominated by SiO_2 and Al_2O_3. Abundances of major elements in the two formations differ from each other. SiO_2 concentrations in the Shanxi Formation range from 52.99% to 63.8%, while they range from 42.21% to 60.23% in the Taiyuan Formation. Most samples from Late Paleozoic shales are in the range of 50.0% to 60.0%. In addition, the average SiO_2 concentration in shale from the Shanxi Formation (58.76%) is higher than that of the Taiyuan Formation (51.62%). However, variations in Al_2O_3 content are different from SiO_2, ranging from 17.39% to 23.98% in the Shanxi Formation and from 15.50% to 36.67% in the Taiyuan Formation, with respective average concentrations of 21.11% and 23.17%. Except for sample XY108 from the Taiyuan Formation, shale samples from the two formations show a negative correlation between SiO_2 and Al_2O_3 (Fig. 5(a)). Among the other major elements, Fe_2O_3 (averaging 6.23%), CaO (0.35%), and Na_2O (0.34%) concentrations are considerably lower than those of SiO_2 and Al_2O_3, and are not correlated with Al_2O_3 (Figs. 5(b), 5 (d) and 5(e)). Average concentrations of MgO, K_2O and P_2O_5 are 0.79%, 2.13% and 0.08%, respectively, and are negatively correlated with Al_2O_3 (Figs. 5(c), 5(f) and 5(h)). TiO_2 contents range between 0.56% and 1.36% and are moderately correlated with Al_2O_3 (Fig. 5(g)) in shale samples from the eastern Ordos Basin.

4.3.2 Trace elements

Trace elements concentrations in Late Paleozoic shale samples from wells LY4 and XY1, are listed in Table 2. The concentration coefficient (CC) (Dai et al., 2015b; Yang et al., 2016) is calculated as the ratio of the concentration of an element in a sample to that of the Upper Continental Crust (UCC) according to a study by McLennan (2001),

Table 1 TOC and major elements concentrations for the late Paleozoic shale (in wt.%)

Samples	Depth/m	TOC	LOI	SiO_2	TiO_2	Al_2O_3	Fe_2O_3	Na_2O	K_2O	CaO	MgO	P_2O_5
LY401	1377.5	1.10	8.78	60.31	0.85	23.98	2.94	0.50	3.02	0.16	0.67	0.04
LY402	1384	1.63	14.09	58.23	0.33	17.39	7.63	0.45	2.28	1.66	1.39	0.06
LY403	1387	1.86	9.75	63.80	0.71	19.41	3.42	0.40	3.01	0.15	0.72	0.05
LY404	1389	6.39	9.07	60.27	0.97	20.55	8.98	0.30	2.41	0.24	1.15	0.13
LY405	1391.5	4.18	11.49	62.19	0.96	20.90	2.71	0.21	1.73	0.11	0.31	0.04
LY406	1430	1.72	20.25	52.10	0.89	22.36	2.97	0.20	1.59	0.15	0.53	0.06
LY407	1433.3	1.99	22.42	50.93	0.84	21.14	3.04	0.18	1.59	0.13	0.49	0.07
LY408	1456	1.27	14.92	51.58	0.84	27.12	4.70	0.18	1.09	0.11	0.28	0.06
LY409	1459	3.34	16.35	46.48	0.80	26.74	10.38	0.20	1.23	0.30	0.59	0.07
LY410	1461.8	3.82	16.33	48.43	0.99	28.81	6.57	0.19	1.16	0.11	0.29	0.06
LY411	1463	1.86	22.34	47.69	1.29	25.04	2.47	0.19	1.08	0.14	0.30	0.04
LY412	1465	1.10	25.46	51.01	1.36	19.04	1.90	0.16	1.53	0.08	0.27	0.03
XY101	1453	3.32	9.15	58.45	0.83	21.72	8.56	0.72	2.96	0.25	1.07	0.11
XY102	1455	2.89	12.88	53.47	0.68	21.62	10.53	0.65	3.39	0.23	0.92	0.11
XY103	1458	1.51	10.01	58.30	0.85	22.31	7.10	0.62	2.47	0.21	1.16	0.08
XY104	1461	1.99	13.61	52.99	0.75	19.43	14.82	0.54	1.90	0.54	1.56	0.10
XY105	1472	2.15	11.79	55.69	0.81	23.24	5.89	0.52	2.69	0.14	0.98	0.07
XY106	1477	4.65	9.22	62.65	1.11	21.62	2.98	0.31	2.25	0.27	0.60	0.05
XY107	1493	4.05	10.61	59.37	0.86	19.46	4.34	0.53	3.72	1.26	0.93	0.12
XY108	1498	4.15	20.19	42.21	0.56	15.50	3.17	0.33	1.97	15.92	1.00	0.06
XY109	1523	2.25	11.54	60.23	0.80	16.75	7.57	0.41	2.06	0.56	0.72	0.19
XY110	1529	3.10	17.70	50.69	1.21	24.90	3.75	0.20	1.78	0.10	0.58	0.05
XY111	1534	2.45	14.75	45.07	1.48	36.67	1.72	0.18	0.28	0.15	0.34	0.07
XY112	1538	2.37	9.61	60.13	1.49	25.19	1.89	0.20	1.64	0.17	0.47	0.04
XY113	1540	2.93	11.88	55.80	0.84	19.52	12.40	0.19	2.60	0.55	1.37	0.15
XY114	1543	4.01	13.90	52.62	0.80	19.36	15.07	0.21	2.28	0.77	1.47	0.16

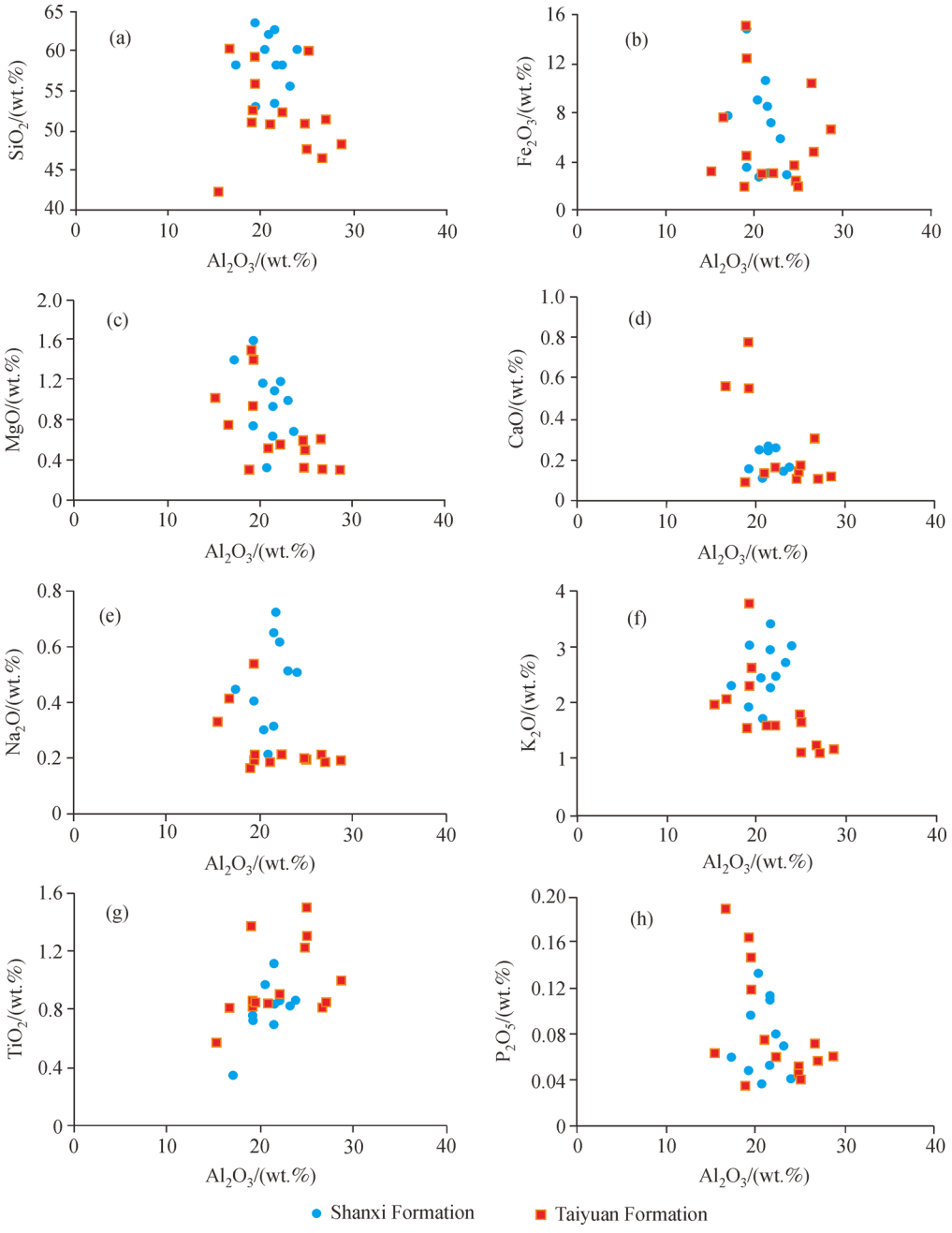

Fig. 5 Major elements plotted against Al_2O_3 for shale samples from the Taiyuan and Shanxi Formations.

and is shown in Fig. 6. Bi and Li are much more abundant with a CC > 2.0, while concentrations of other elements vary across different shale samples from the two wells. Different lithofacies in the Shanxi and Taiyuan Formations show similar trace elements concentrations. Black shale from the Shanxi Formation at well LY4 is characterized by CC values of Cs > Li > Cu > Ba > Rb > V > Sr > Cr > Co > Ni, except for LY404 and LY405 (Fig. 6(a)). For samples from well XY1 in the Shanxi Formation, CCs are Li > Cs > Cu > V > Ba > Rb > Co > Cr > Ni > Sr (Fig. 6 (b)). Organic-rich shale from the Taiyuan Formation shows CCs of Li > Cu > Cs > V > Co > Cr > Ni > Ba > Rb > Sr in well LY4 (Fig. 6(c)), and Li > Cs > V > Cu > Cr > Co > Rb > Sr > Ni > Ba at well XY1 (Fig. 6(d)).

4.3.3 Rare earth elements

The concentrations of rare earth elements (REEs) in Late Paleozoic shale samples from wells LY4 and XY1 are shown in Table 3. REE concentrations range from

Table 2 Trace elements concentrations ($\times 10^{-6}$) for shale from the eastern Ordos Basin, China

Samples	Li	Be	Sc	V	Cr	Co	Ni	Cu	Zn	Ga	Rb	Sr	Zr	Nb	Cs	Ba	Hf	Ta	Tl	Pb	Bi	Th	U
LY401	50.0	3.30	13.7	73.0	53.3	3.53	11.6	22.8	71.5	34.1	150.0	166.0	310	29.7	17.4	687	9.21	2.03	0.97	19.8	0.49	18.4	3.77
LY402	31.8	2.12	8.8	49.4	23.7	6.58	15.5	79.3	83.5	22.0	84.6	226.0	184	16.0	5.85	573	5.96	1.21	0.61	33.0	0.44	13.2	3.08
LY403	36.1	2.84	17.0	109.0	61.9	14.0	18.5	35.0	98.0	28.4	147.0	174.0	283	23.0	12.5	704	7.96	1.51	0.92	28.8	0.43	18.7	4.64
LY404	43.0	1.46	17.8	94.5	89.2	14.8	28.1	40.8	158.0	33.6	125.0	189.0	361	32.7	8.19	573	11.0	2.18	0.83	35.2	0.48	24.2	5.71
LY405	59.5	2.39	15.9	84.5	64.9	5.14	10.9	24.7	115.0	26.7	80.8	82.2	274	28.0	6.22	354	8.52	1.74	0.55	33.9	0.31	20.2	4.35
LY406	89.2	2.05	16.4	85.1	54.9	9.78	24.2	31.3	76.0	26.7	69.4	102.0	186	20.5	6.77	255	5.54	1.36	0.65	23.9	0.34	17.1	4.04
LY407	81.1	2.45	17.1	111.0	56.9	12.3	23.7	32.6	111.0	27.2	69.9	125.0	209	20.3	6.30	263	6.53	1.38	0.72	26.5	0.39	18.0	4.58
LY408	111.0	1.77	19.2	106.0	59.2	17.7	21.9	24.3	59.4	31.3	42.2	99.6	259	20.8	2.94	132	8.89	1.34	0.60	43.8	0.44	20.1	6.54
LY409	100.0	2.33	20.5	128.0	60.6	16.5	20.0	16.8	25.0	30.9	45.7	144.0	229	18.9	3.07	149	7.89	1.21	0.39	18.1	0.44	19.6	5.96
LY410	112.0	2.90	19.9	95.9	61.6	20.5	31.3	75.3	48.0	33.3	44.1	128.0	270	20.9	4.51	181	9.10	1.61	0.61	30.1	0.45	21.1	3.98
LY411	184.0	3.39	17.0	69.3	54.3	3.91	12.9	70.0	46.5	39.7	37.7	70.5	322	31.9	4.16	152	8.94	2.09	0.30	26.7	0.68	23.5	4.57
LY412	83.6	3.85	12.2	68.2	57.1	9.22	15.5	63.2	49.2	32.6	54.4	63.5	226	31.6	6.68	188	6.73	1.98	0.28	20.6	0.19	18.9	-
XY101	43.3	3.75	17.2	103.0	56.4	10.5	22.5	33.7	128.0	33.0	132.0	181.0	283	28.0	7.47	643	8.02	1.73	0.64	33.4	0.47	21.6	4.79
XY102	38.0	3.89	17.4	141.0	54.7	37.0	54.8	44.3	169.0	30.3	156.0	190.0	320	22.4	12.1	748	7.84	1.40	1.29	43.7	0.66	21.4	5.48
XY103	59.0	3.86	17.4	116.0	64.9	18.5	33.6	35.0	143.0	29.5	118.0	189.0	325	25.7	8.52	639	8.61	1.55	0.70	34.1	0.46	19.7	5.46
XY104	54.2	3.86	18.9	173.0	87.0	9.88	45.0	27.4	168.0	24.9	98.9	243.0	285	20.4	8.97	664	7.75	1.19	0.77	21.8	0.58	18.6	10.9
XY105	67.9	3.70	19.0	151.0	73.2	15.1	40.9	28.6	180.0	31.6	117.0	193.0	311	25.5	6.70	469	9.19	1.52	0.74	24.4	0.68	21.0	6.09
XY106	69.9	3.02	16.2	101.0	70.2	5.62	14.1	16.1	52.6	29.1	90.9	111.0	216	25.3	5.78	380	6.43	1.54	0.51	27.0	0.20	16.6	4.91
XY107	36.8	2.54	15.0	91.6	59.8	18.4	26.3	22.9	90.5	26.8	120.0	253.0	156	18.0	4.57	391	4.67	1.20	0.67	31.4	0.28	15.6	3.55
XY108	39.5	1.69	10.0	69.6	43.5	9.60	31.0	15.1	89.9	16.1	60.9	113.0	133	15.2	3.42	252	3.93	0.91	0.26	25.1	0.19	12.3	3.98
XY109	43.8	2.33	12.2	100.0	59.0	8.11	14.2	24.0	104.0	23.8	79.0	132.0	175	15.5	4.68	217	4.19	0.92	0.87	23.7	0.29	11.1	2.67
XY110	145.0	3.14	22.6	190.0	144.0	16.3	41.2	35.2	119.0	27.6	77.8	85.6	162	20.0	10.6	328	4.68	0.15	0.46	28.5	0.55	17.5	4.82
XY111	514.0	1.98	19.1	147.0	168.0	14.2	63.7	47.4	67.1	47.0	12.9	86.5	288	42.5	1.83	108	8.29	2.80	0.10	19.5	0.99	28.1	7.03
XY112	92.5	2.76	20.9	174.0	112.0	2.25	11.7	12.9	37.5	34.1	75.3	85.0	249	26.1	8.25	225	7.59	1.57	0.42	10.6	0.34	17.9	5.11
XY113	77.4	3.80	18.7	132.0	80.2	11.9	25.1	38.5	128.0	27.9	122.0	125.0	179	17.5	9.53	292	4.88	1.19	0.55	19.2	0.52	15.6	3.61
XY114	94.7	3.31	17.7	124.0	80.0	27.2	38.8	31.5	173.0	26.3	110.0	120.0	177	17.1	9.48	276	4.98	1.16	0.46	23.3	0.53	15.0	3.86

232.7 $\times 10^{-6}$ to 427.4 $\times 10^{-6}$ at well LY4, and from 150.3 $\times 10^{-6}$ to 434.1 $\times 10^{-6}$ at well XY1. Based on the Post Archean Australian Sedimentary Rocks (PAAS)-normalized REE patterns (PAAS-normalized REE value = REE contents in samples/REE contents in PAAS), most samples from the Shanxi Formation have flat REE patterns (LaN/YbN: 0.93–1.19, average of 1.08) with very weak negative Ce anomalies (Ce/Ce*: 0.89–0.85, except for 1.30 in sample LY403) and significantly negative Eu anomalies (Eu/Eu*: 0.67–0.91) (Fig. 7(a)). The Taiyuan Formation samples from well LY4 are characterized by strongly negative Ce anomalies (Ce/Ce*: 0.84–1.40, average of 1.21) and light REE (LREE) enrichment (LaN/YbN: 0.90–1.50, average of 1.17) (Fig. 7(b)). With a slight LREE enrichment (LaN/YbN: 1.10–1.43, average of 1.20), the REE distribution patterns in the Shanxi Formation at well XY1 are anomalously depleted in Eu with Eu/Eu*: 0.69—0.84, except for a value of 1.03 in sample XY104 (Fig. 7(c)). The REE patterns of shale samples from the Taiyuan Formation exhibit the same characteristics as those from the Shanxi Formation at well XY1 (Fig. 7(d)).

5 Discussion

Variations in paleoenvironments and paleoclimate are responsible for different redox conditions, which in turn influence element concentrations in shale (Li et al., 2019b). In addition, because shale TOC is affected by paleoclimate and paleoenvironment, there may be a relationship between trace elements indicators and TOC. Based on prior studies (Hakimi et al., 2013; Dai et al., 2014; Dai et al., 2015a; Sarki Yandoka et al., 2015; Zhang et al., 2016) and geochemical data, including mineralogy, major elements, trace elements, and REEs, we describe origin of the shales, as well as the paleoenvironment, paleoclimate and sedimentary conditions that prevailed during shale formation. In addition, we investigate the relationships between TOC and trace elements.

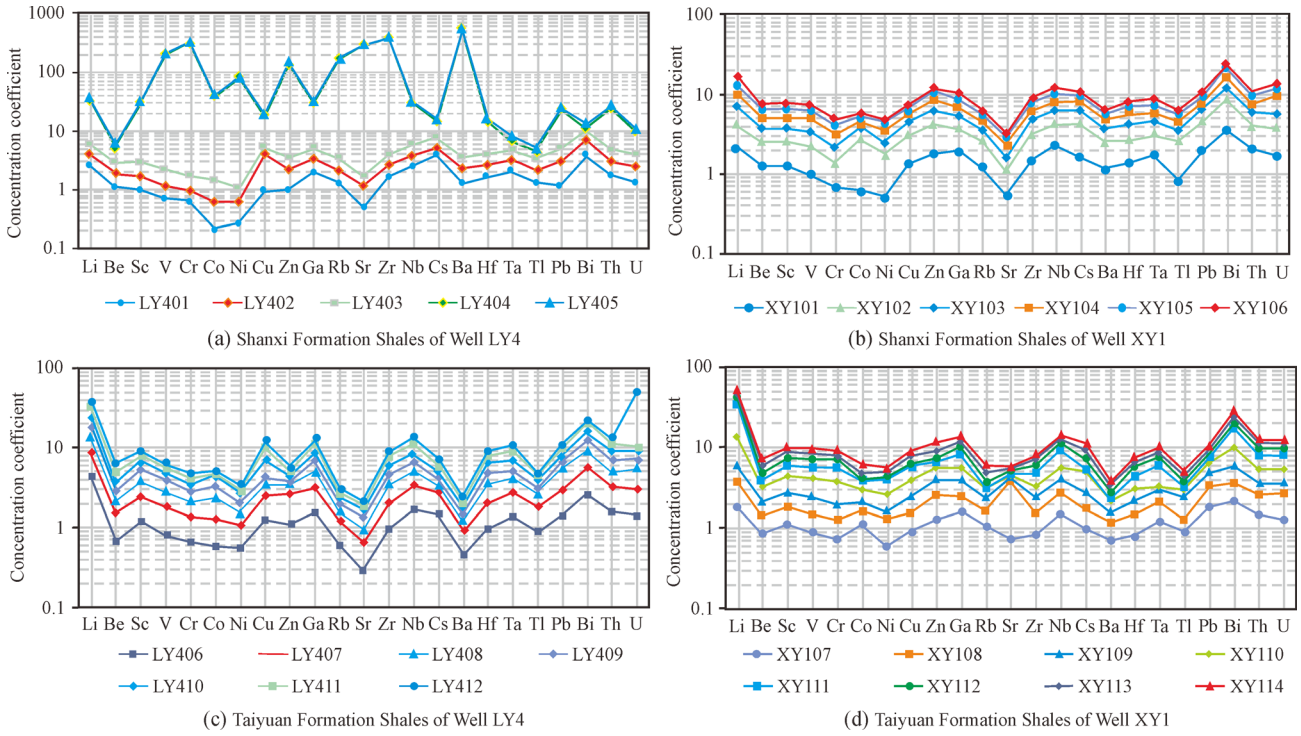

Fig. 6 Concentration coefficients of trace elements relative to Upper Continental Crust (from McLennan (2001)) for Taiyuan and Shanxi Formation shales from wells LY4 and XY1, eastern Ordos Basin, China.

5.1 Provenance of the transitional shales

Identifying the provenance of sedimentary rock samples typically involves studying the geochemistry of clastic sediments, such as Al_2O_3/TiO_2 and TiO_2/Zr ratios. Al_2O_3/TiO_2 ratios for mafic, intermediate, and felsic igneous rocks commonly range between 3 and 8, 8 and 21, and 21 and 70, respectively (Hayashi et al., 1997). The Al_2O_3/TiO_2 ratios for shale samples in this study range from 14 to 52.07, with an average of 24.87 (Fig. 8), suggesting felsic igneous rock was dominant in the source area. TiO_2/Zr ratios decrease from >200 for mafic rocks to 199 to 55 for intermediate rocks, and to less than 55 for felsic igneous rocks (Hayashi et al., 1997). TiO_2/Zr ratios of our samples vary from 18.15 to 59.84 (average of 39.46) (Fig. 9), suggesting a felsic source, which is in agreement with observed Al_2O_3/TiO_2 ratios.

Among the known weathering/alteration indices, the Chemical Index of Alteration (CIA) is a well-established method for quantifying the degree of source weathering (Nesbitt and Young, 1982). Source weathering and elemental redistribution during diagenesis can also be assessed using the Chemical Index of Weathering (CIW). High CIA and CIW values often indicate strong weathering in the source region. The CIA values range from 73.78 to 98.14 with an average of 86.95, which, together with CIW values, indicates intense chemical weathering in the source area. The mobility of elements was evaluated using a Al_2O_3-CaO^*+Na_2O-K_2O (A-CN-K) ternary diagram (where CaO^* indicates the CaO in silicate phase) (Nesbitt and Young, 1984), in which the shale samples plot above the plagioclase-potash feldspar joint (Fig. 10), suggesting the shale samples were not subjected to potassium metasomatism during diagenesis.

5.2 Paleoclimate

The C-value (C-value = (Fe + Mn + Cr + Ni + V + Co)/(Ca + Mg + K + Na + Sr + Ba), measured in $\times 10^{-6}$) of shale was used to identify climate conditions. C-values varied from 0.2 $\times 10^{-6}$ to 4.5 $\times 10^{-6}$, with most samples in the range of 0.4 $\times 10^{-6}$ to 2.2 $\times 10^{-6}$. In a CIW- C-value diagram (Fig. 11), most of the data indicate a humid climate, except for a few samples in that fall in the semi-arid, and semi-arid to semi-humid range.

The Sr/Cu ratio is typically used to reflect paleoclimate conditions. A warm-humid climate is indicated by Sr/Cu ratios between 1.3 and 5.0, whereas Sr/Cu ratios higher than 5.0 indicate a dry-hot climate (Tao et al., 2016). The Sr/Cu values for shale samples range between 1.00 and 11.05, with an average of 4.85, indicating a warm-humid climate.

The Sr/Ba ratio is a good indicator of depositional water conditions (Meng et al., 2012). Sr/Ba ratios of the shale samples vary from 0.23 to 0.97, falling within the fresh water and mixed water ranges (Figs. 12 and 13) that

Table 3 Rare earth elements concentrations ($\times 10^{-6}$) and relative ratios for shale from the eastern Ordos Basin, China

Well	Samples	La	Ce	Pr	Nd	Sm	Eu	Gd	Tb	Dy	Ho	Er	Tm	Yb	Lu	Y	LREE	HREE	REE	LREE/HREE
LY4	LY401	59.1	111	13.5	51.0	8.65	1.21	6.49	1.13	6.01	1.22	3.53	0.61	4.25	0.551	33.3	244.5	23.8	268.3	10.3
	LY402	51.5	99	11.5	41.4	7.53	0.99	6.24	1.14	5.86	1.23	3.39	0.65	4.10	0.607	32.9	211.5	23.2	234.7	9.1
	LY403	75.5	136	15.0	50.1	7.39	1.00	6.07	1.11	6.22	1.29	3.66	0.74	4.66	0.676	33.4	285.0	24.4	309.4	11.7
	LY404	96.3	177	20.8	78.0	14.4	2.50	11.3	1.94	9.96	1.99	5.11	0.98	6.29	0.792	51.9	389.0	38.4	427.4	10.1
	LY405	54.0	101	11.9	44.1	8.16	1.26	6.35	1.13	6.13	1.15	2.95	0.50	3.49	0.412	29.8	220.4	22.1	242.5	10.0
	LY406	69.3	132	14.4	51.7	8.28	1.52	6.47	1.06	5.71	1.23	3.15	0.55	3.92	0.540	30.9	277.2	22.6	299.8	12.3
	LY407	78.1	153	16.8	61.8	10.1	1.95	7.67	1.29	6.87	1.29	3.89	0.67	4.71	0.615	36.6	321.8	27.0	348.8	11.9
	LY408	90.5	162	17.8	60.4	7.94	1.23	6.97	1.29	7.88	1.70	4.74	0.89	5.85	0.818	42.4	339.9	30.1	370.0	11.3
	LY409	88.8	165	19.6	75.4	13.8	3.74	11.5	1.79	9.38	1.83	5.20	0.83	6.72	0.991	52.7	366.3	38.2	404.6	9.6
	LY410	83.4	154	17.5	62.1	8.83	1.15	6.29	1.21	7.07	1.51	4.16	0.74	5.46	0.687	39.1	327.0	27.1	354.1	12.1
	LY411	60.4	101	10.5	32.0	4.90	0.69	4.62	1.11	6.48	1.27	3.39	0.71	4.97	0.704	34.7	209.5	23.3	232.7	9.0
	LY412	65.0	109	11.8	39.0	6.02	0.76	4.73	0.89	4.52	0.89	2.56	0.45	3.19	0.478	22.7	231.6	17.7	249.3	13.1
XY1	XY101	83.4	155	17.4	62.9	10.5	1.60	8.92	1.52	8.19	1.61	4.69	0.84	5.34	0.711	47.1	330.8	31.8	362.6	10.4
	XY102	85.3	154	16.5	56.9	9.01	1.26	8.15	1.40	7.92	1.63	4.72	0.86	5.35	0.721	44.6	322.9	30.8	353.7	10.5
	XY103	84.6	167	19.4	76.7	14.7	2.28	11.30	1.92	9.64	1.82	5.19	0.90	5.49	0.73	52.9	364.7	37.0	401.7	9.9
	XY104	92.4	181	20.8	80.7	15.0	3.02	12.40	2.15	10.8	2.03	5.74	0.99	6.21	0.829	63.7	392.9	41.2	434.1	9.6
	XY105	87.1	164	18.4	68.8	12.0	1.99	10.10	1.78	9.40	1.78	5.05	0.86	5.17	0.679	49.8	352.3	34.8	387.1	10.1
	XY106	53.9	101	10.8	38.6	6.22	1.06	5.55	0.92	4.82	0.96	2.72	0.46	2.78	0.394	25.2	211.6	18.6	230.2	11.4
	XY107	63.7	118	13.0	47.5	7.77	1.38	6.18	0.95	4.86	0.97	3.03	0.50	3.05	0.409	26.5	251.4	20.0	271.3	12.6
	XY108	40.3	68	7.8	27.8	4.39	0.68	3.79	0.63	3.48	0.71	2.14	0.38	2.32	0.314	21.8	148.7	13.8	162.5	10.8
	XY109	47.6	92	10.0	37.2	6.34	1.21	5.48	0.89	4.74	0.92	2.82	0.50	3.11	0.437	27.3	194.1	18.9	213.0	10.3
	XY110	50.5	107	11.6	45.0	8.57	1.62	6.47	1.05	5.31	1.01	2.96	0.53	3.34	0.458	27.3	224.3	21.1	245.4	10.6
	XY111	32.0	59	6.9	26.1	5.35	1.14	4.50	0.86	5.20	1.05	3.08	0.59	3.74	0.510	30.7	130.8	19.5	150.3	6.7
	XY112	33.4	60	7.1	26.5	5.06	1.07	4.51	0.87	4.78	0.90	2.56	0.44	2.81	0.378	25.3	133.4	17.3	150.7	7.7
	XY113	55.1	108	12	45.6	8.12	1.49	7.21	1.22	6.43	1.26	3.69	0.647	3.99	0.533	35.9	230.3	25.0	255.3	9.2
	XY114	48.9	98.7	10.7	40.9	7.63	1.57	6.98	1.16	6.08	1.19	3.45	0.599	3.62	0.482	34.6	208.4	23.6	232.0	8.9

indicate terrestrial and transitional depositional environments.

The CIA can also reflect paleoclimatic conditions: when the CIA is in the range of 50–65, it is indicative of a cold and dry climate with little chemical weathering. When the CIA ranges between 65 and 85, it indicates a warm and humid climate with moderate chemical weathering. Finally, a CIA between 85 and 100 indicates a hot and humid climate with strong chemical weathering (Nesbitt and Young, 1982; McLennan, 1993). The CIA values of the shale samples indicate deposition in a hot-humid climate. In addition, clay minerals are mainly composed of kaolinite and I/S mixed layers, suggesting that the paleoclimate was humid during the late Paleozoic period.

In summary, different indicators (C-value, Sr/Cu, CIA) suggest that the shales of the Shanxi and Taiyuan Formations from the eastern Ordos Basin were deposited in a hot-humid climate in terrestrial and transitional environments during the Late Paleozoic period.

5.3 Redox conditions constrained from trace elements

The sedimentary accumulation of trace elements may occur during deposition of various mineral phases such as metal sulfides insoluble oxides and oxyhydroxides, phosphate and sulfate minerals, organometallic complexes, or adsorbed onto organic or mineral surfaces. Following deposition, the behavior of different trace elements is highly variable during diagenesis, depending on conditions in the subsurface environment. Uranium (U), vanadium (V) and molybdenum (Mo) are redox proxies with minimal detrital influence, whereas chromium (Cr) and cobalt (Co) are strongly influenced by detrital material (Fu et al., 2011a; Li et al., 2015; Ma et al., 2015). As a result, trace elements such as U, V, Ni, Co, and Th, are generally considered to be redox-sensitive and exhibit similar geochemical behavior (Algeo and Maynard, 2004; Tribovillard et al., 2006). Therefore, the ratios of these elements, (V/Cr, Ni/Co, V/(V + Ni) and U/Th) can be used to

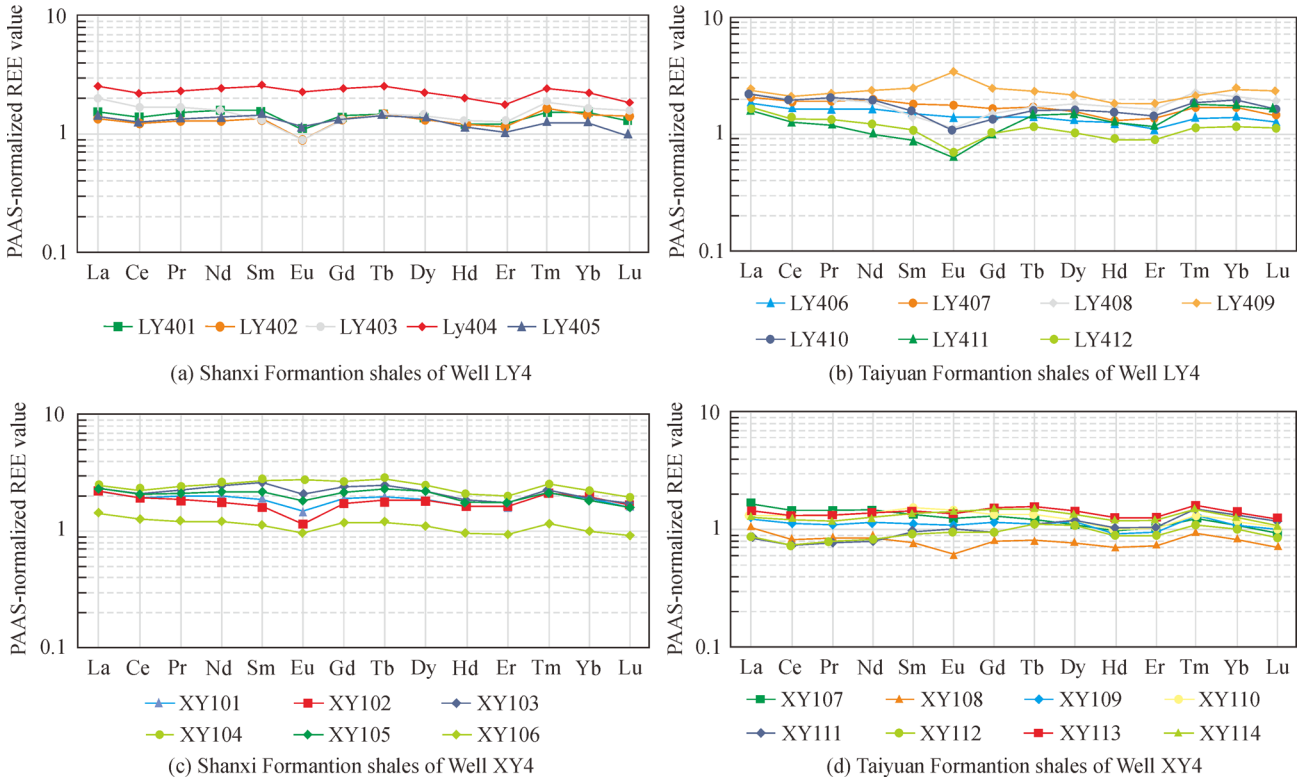

Fig. 7 PAAS-normalized REE patterns of shale samples from the Shanxi and Taiyuan Formations from wells LY4 and XY1, eastern Ordos Basin, China.

investigate redox conditions within sediments (Table 4).

High Al content is typically thought to be caused by greater terrestrial influx, while increased Fe concentrations generally indicate influence of hydrothermal processes (Udchachon et al., 2017). The $Al_2O_3/(Al_2O_3+Fe_2O_3)$ ratios for the samples in this study range from 0.56 to 0.93, indicating that shale was deposited in a continental margin setting (Murray, 1994).

The V/Cr relationship reflects the degree of oxidation–reduction and is a proxy for sea level variability. A V/Cr ratio greater than 4.25 indicates an anoxic environment, while ratios between 2.00 to 4.25 indicate a suboxic to dysoxic depositional environment, and ratios less than 2.00 indicate an oxic environment (Jones and Manning, 1994). The V/Cr ratios of the shale samples range from 0.88 to 2.58 with an average of 1.63, suggesting deposition in an oxic to suboxic environment. The different formations present in the two wells show small differences in V/Cr values. In well LY4, V/Cr ratios for the Shanxi Formation

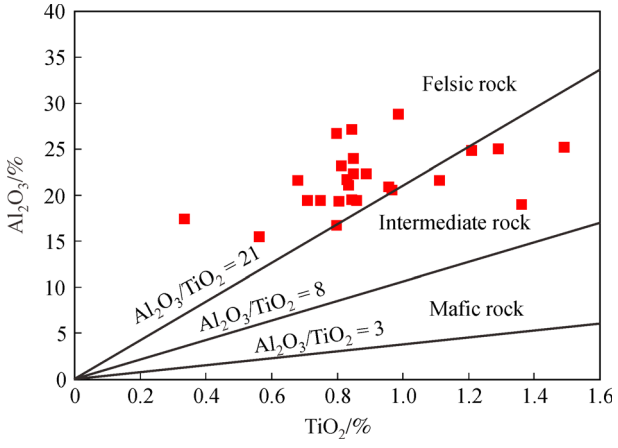

Fig. 8 Plot of Al_2O_3 vs. TiO_2 for Late Paleozoic shales from the eastern Ordos Basin.

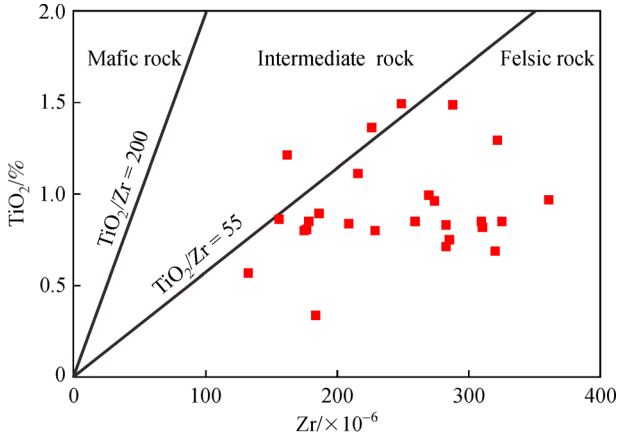

Fig. 9 Plot of TiO_2 vs. Zr for Late Paleozoic shales from the eastern Ordos Basin.

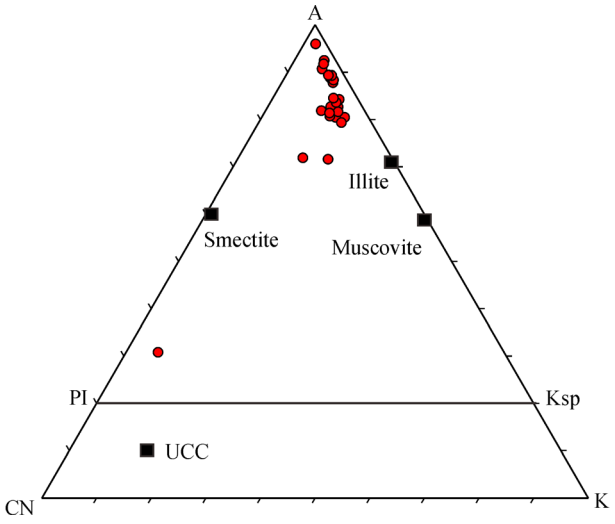

Fig. 10 A-CN-K ternary diagram for shale samples from the eastern Ordos Basin. Mineral compositions: Pl, plagioclase; Ksp, K-feldspar; UCC, Upper Continental Crust; A, Al_2O_3; CN, $CaO^* + Na_2O$; K, K_2O.

are slightly higher than those for the Taiyuan Formation, while the same ratios were slightly lower in the Shanxi Formation in well XY1. These small differences between two formations and wells likely indicate sea level fluctuation during shale deposition.

A Ni/Co ratio below 5.0 indicates oxic depositional conditions, suboxic to dysoxic conditions between 5.0 and 7.0, and anoxic conditions above 7.0 (Jones and Manning, 1994). Except for sample XY112, the Ni/Co ratios of the shale samples range from 1.21 to 5.20, with an average of 2.37, suggesting that Late Paleozoic shale in the study area was deposited in an oxic environment with very little fluctuation in redox conditions.

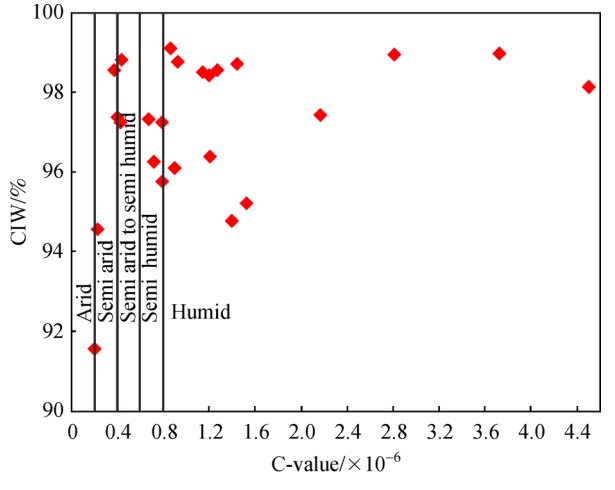

Fig. 11 CIW– C-value diagram for Taiyuan and Shanxi Formations shale samples. CIW, chemical indices of weathering; C-value, $(Fe + Mn + Cr + Ni + V + Co)/(Ca + Mg + K + Na + Sr + Ba)$, $\times 10^{-6}$.

High values for $V/(V + Ni)$ ratios suggest strongly euxinic depositional conditions (Arthur and Sageman, 1994). Ratios below 0.6 indicate oxic conditions, values between 0.6 and 0.85 represent dysoxic conditions, and values greater than 0.85 represent suboxic (anoxic) conditions. The $V/(V + Ni)$ ratios for shale samples in this study range from 0.69 to 0.94 with an average of 0.81, indicating that the majority of samples were deposited under dysoxic conditions.

Th is one of the detrital components that is unaffected by changes in redox conditions, while organic-bound U is considered to be sensitive to changing redox conditions. U/Th ratios greater than 1.25 indicate anoxic conditions, ratios between 0.75 and 1.25 indicate suboxic to dysoxic conditions, and ratios below 0.75 represent oxic conditions. U/Th ratios for shale samples from wells LY4 and XY1 are between 0.19 and 0.33, with an average of 0.27, indicating oxic conditions. Most samples from the Taiyuan Formation fall within the dysoxic range, while samples from the Shanxi Formation are in the oxic range, suggesting a shift from a humid depositional environment to a terrestrial, arid environment.

In general, V/Cr, Ni/Co, $V/(V + Ni)$ and U/Th ratios decrease with increasing oxygenation levels in a water column (Wang et al., 2015). Overall, based on redox sensitive enrichment factors and ratios, we conclude that redox conditions during Late Paleozoic shale deposition in the Shanxi and Taiyuan Formations were mainly dysoxic to oxic with small-scale variations due to fluctuations in climate and water level within a transitional sedimentary environment.

5.4 Rare earth element variations of different formations

Rare Earth Elements (REEs) have special geochemical characteristics such as extremely similar chemical properties and low solubility (Bai et al., 2015), as well as geochemical stability during weathering, erosion, transportation and deposition (Fu et al., 2011a). REEs, which typically originate from plants, seawater, and terrigenous substances are often used to trace sediment source in a depositional basin. Ce anomalies can be used as a signature for the presence of seawater, as seawater is enriched both LREEs and HREEs (Birk and White, 1991). Shale samples in this study show small Ce anomalies and low LREE and HREE enrichment (Table 3), indicating that seawater was not a source of REEs in the study area.

REE patterns can also indicate the source of sedimentary rocks (McLennan, 1993). Generally, mafic rocks have lower LREE/HREE ratios and no Eu anomalies, while felsic rocks have higher LREE/HREE ratios and negative Eu anomalies. The PAAS-normalized REE patterns indicate that all shale samples are characterized by LREE enrichment, HREE deficiencies and Eu anomalies. Ratios of $(La/Yb)_N$ (Table 3, Fig. 13), which can be used in place

of LREE/HREE ratios, suggest that Late Paleozoic shale in the study area was sourced from felsic rock.

Ce and Eu anomalies are considered to be effective redox indicators for shale sedimentary environments (Tribovillard et al., 2006). Ce anomalies in ancient sediments are effective tracers of secular variations in redox conditions and are determined from the mixing ratio of authigenic minerals, detrital terrigenous minerals, and biogenic silica. Positive and negative Ce anomalies are indicative of terrigenous input and an oxic environment, respectively (Han et al., 2015). The weak negative Ce anomalies found in this study and the vertical variability of Ce/Ce* (Fig. 13) indicate an oxic depositional environment with terrigenous input.

Positive Eu anomalies are commonly found in extremely reducing hydrothermal fluids that favor reduction of Eu^{3+} to Eu^{2+} and are very common in marine hydrothermal sediments (Olivarez and Owen, 1991; Douville et al., 1999; Xiong et al., 2019; Yang et al., 2019). Previous research has shown that Eu anomalies in marine shale from south China provide some evidence of hydrothermal inputs. In this study, shale samples exhibite LREE enrichment with negative Eu anomalies (Fig. 6, Tables 3 and 4), suggesting that the Shanxi and Taiyuan Formations were affected by detrital inputs rather than hydrothermal activity.

5.5 Relationship between TOC and trace elements

The geochemical composition of shale is clearly affected by the abundance of organic matter (He et al., 2018; Tang et al., 2019; He et al., 2020). The TOC variability in the samples is consistent with Sr/Ba and Sr/Cu ratios, especially in samples from well LY4 (Fig. 12), which suggests that the abundance of organic matter is influenced by climate and water conditions. From bottom to top,

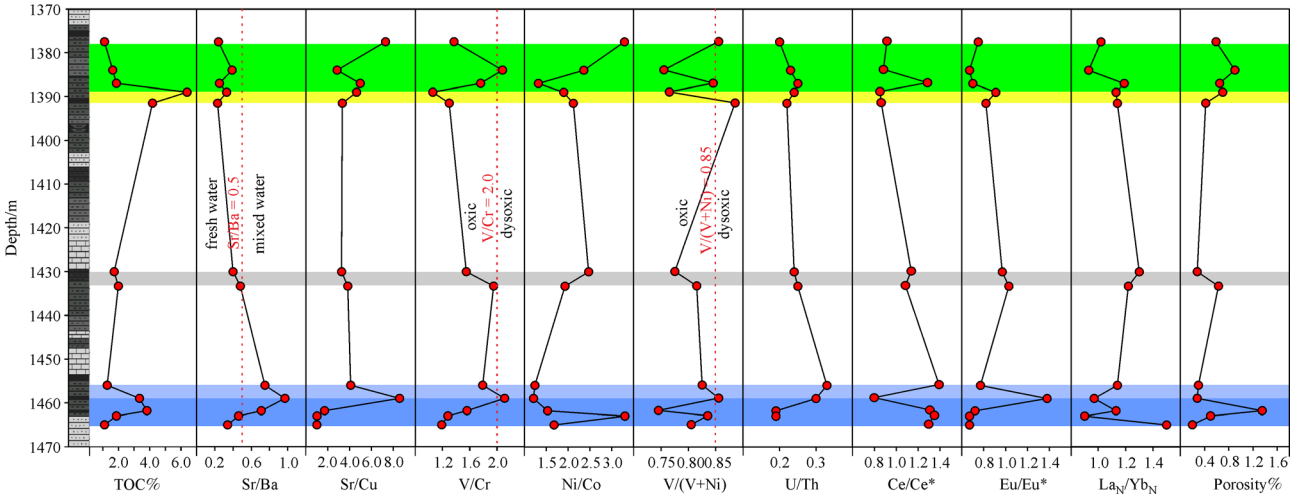

Fig. 12 Stratigraphic profiles of geochemical indicators from well LY4.

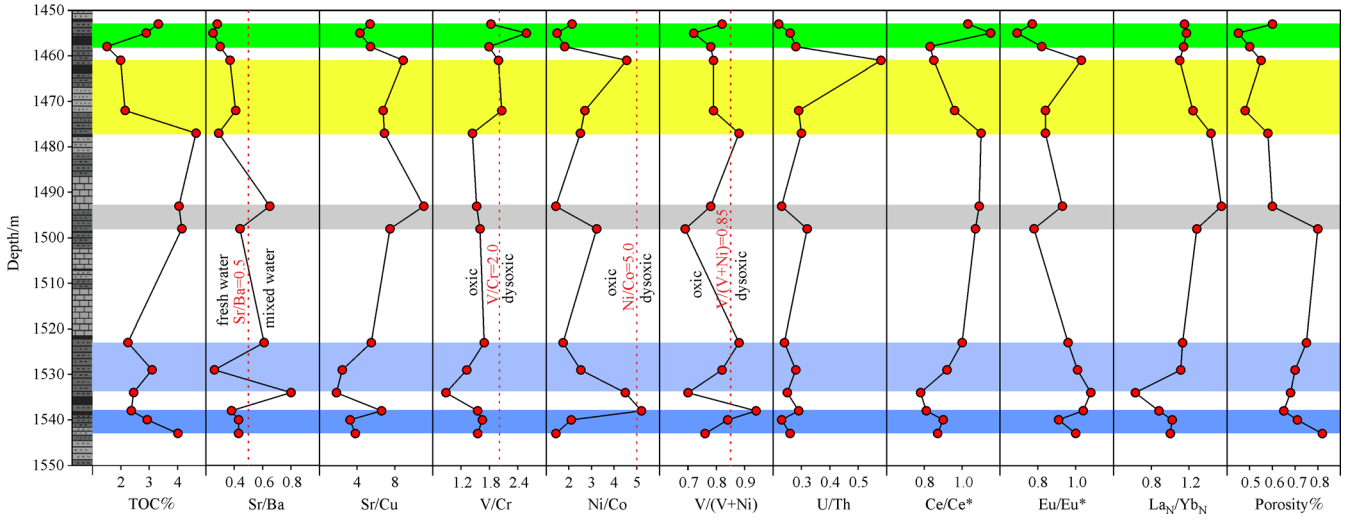

Fig. 13 Stratigraphic profiles of geochemical indicators from well XY1.

Table 4 Selected geochemical indicators for shale from the eastern Ordos Basin, China (%)

Samples	CIA*	CIW*	C-value	Sr/Ba	Sr/Cu	Al_2O_3/TiO_2	V/Cr	Ni/Co	V/(V + Ni)	U/Th	Ce/Ce*	Eu/Eu*	La_N/Yb_N
LY401	84.84	97.32	0.67	0.24	7.28	28.28	1.37	3.29	0.86	0.20	0.95	0.75	1.02
LY402	74.08	89.19	1.31	0.39	2.85	52.07	2.08	2.36	0.76	0.23	0.92	0.67	0.93
LY403	82.64	97.24	0.79	0.25	4.97	27.38	1.76	1.32	0.85	0.25	1.30	0.70	1.19
LY404	86.45	97.44	2.17	0.33	4.63	21.25	1.06	1.90	0.77	0.24	0.89	0.91	1.13
LY405	89.98	98.51	1.14	0.23	3.33	21.84	1.30	2.12	0.89	0.22	0.90	0.82	1.14
LY406	91.05	98.42	1.20	0.40	3.26	25.21	1.55	2.47	0.78	0.24	1.16	0.97	1.30
LY407	91.03	98.54	1.27	0.48	3.83	25.32	1.95	1.93	0.82	0.25	1.11	1.03	1.22
LY408	94.62	98.95	2.81	0.75	4.10	32.13	1.79	1.24	0.83	0.33	1.40	0.77	1.14
LY409	92.88	98.14	4.50	0.97	8.57	33.55	2.11	1.21	0.86	0.30	0.84	1.38	0.97
LY410	94.65	98.97	3.72	0.71	1.70	29.19	1.56	1.53	0.75	0.19	1.32	0.72	1.13
LY411	93.91	98.72	1.44	0.46	1.01	19.41	1.28	3.30	0.84	0.19	1.36	0.67	0.90
LY412	90.55	98.76	0.93	0.34	1.00	14.00	1.19	1.68	0.81	-	1.31	0.67	1.50
XY101	82.65	95.76	0.79	0.28	5.37	26.17	1.83	2.14	0.82	0.22	1.03	0.77	1.15
XY102	81.54	96.10	0.90	0.25	4.29	31.75	2.58	1.48	0.72	0.26	1.15	0.69	1.17
XY103	84.93	96.26	0.72	0.30	5.40	26.31	1.79	1.82	0.78	0.28	0.83	0.82	1.14
XY104	84.06	94.77	1.40	0.37	8.87	25.98	1.99	4.55	0.79	0.58	0.85	1.03	1.10
XY105	85.79	97.26	0.43	0.41	6.75	28.62	2.06	2.71	0.79	0.29	0.96	0.84	1.24
XY106	86.72	97.39	0.40	0.29	6.89	19.48	1.44	2.51	0.88	0.30	1.10	0.84	1.43
XY107	73.78	91.56	0.20	0.65	11.05	22.68	1.53	1.43	0.78	0.23	1.09	0.93	1.54
XY108	83.00	48.82	0.06	0.44	7.48	27.53	1.60	3.23	0.69	0.32	1.07	0.78	1.28
XY109	82.89	94.57	0.23	0.61	5.50	20.99	1.69	1.75	0.88	0.24	1.00	0.96	1.13
XY110	91.50	98.82	0.44	0.26	2.43	20.58	1.32	2.53	0.82	0.28	0.92	1.01	1.11
XY111	98.14	99.11	0.86	0.80	1.82	24.78	0.88	4.49	0.70	0.25	0.78	1.08	0.63
XY112	91.55	98.54	0.37	0.38	6.59	16.91	1.55	5.20	0.94	0.29	0.81	1.04	0.88
XY113	83.82	96.38	1.21	0.43	3.25	23.13	1.65	2.11	0.84	0.23	0.90	0.91	1.02
XY114	83.55	95.22	1.52	0.43	3.81	24.08	1.55	1.43	0.76	0.26	0.87	1.00	1.00

Notes: CIA*, chemical index of alteration, $CIA^* = [Al_2O_3/(Al_2O_3 + CaO^* + Na_2O + K_2O)]\times 100$ (Nesbitt and Young, 1982); CIW, chemical indices of weathering, $CIW = [Al_2O_3/(Al_2O_3 + CaO^* + Na_2O)]\times 100$. CaO*, CaO in silicate phase (to calculate CaO*, the assumption proposed by McLennan (1993) was followed).

under regressive conditions, the paleoenvironment shifted from dysoxic to oxic, and aqueous conditions changed from mixed water to fresh water. At depths between 1450 m and 1470 m, mixed water conditions and a warm-humid environment (indicated by Sr/Ba, Sr/Cu, V/Cr and U/Th ratios in Fig. 12) resulted in increasing TOC abundance. At depths between 1375 m and 1390 m, oxic fresh water conditions with abundant TOC deposition prevailed as the ratios of Sr/Ba and U/Th decreased. At well XY1, at depths between 1450 m and 1480 m, TOC abundance and Sr/Cu ratios show a similar vertical variability (Fig. 13).

Therefore, it can be concluded that a warm-humid and mixed water environment was present during the deposition of abundant organic matter in the shales, while oxic conditions did not favor the preservation of organic matter.

6 Conclusions

Based on the analysis of TOC abundance, as well as mineral, and elemental compositions, a detailed study of Late Paleozoic shale from the Ordos Basin was conducted.

Dominant minerals in the studied samples are quartz and clay, while major and trace elements show differences in distribution between the Shanxi and Taiyuan Formations across the two wells. Total organic carbon values of the samples range from 1.10% to 4.65%, with high thermal maturity (average R_o value of 2.85). Vertical variability is consistent with Sr/Cu, Sr/Ba, V/Cr and U/Th ratios, suggesting that humid-warm, dysoxic-oxic environments preserved more organic matter.

C-values, together with Sr/Cu ratios, suggest that the paleoclimate in the study area was relatively humid during the Late Paleozoic period. High Al contents and $Al_2O_3/(Al_2O_3 + Fe_2O_3)$ ratios indicate that the shales were deposited in a continental margin setting, while trace element redox indices, such as V/Cr, Ni/Co, V/(V + Ni) and U/Th, suggest that shale was deposited in a transitional sedimentary environment under dysoxic to oxic conditions during the Late Paleozoic period.

Al_2O_3/TiO_2 and TiO_2/Zr ratios of the shale samples indicate that felsic igneous rocks were dominant in the source area. Values of CIA and CIW for the shale samples suggest intense chemical weathering in the source area and the A-CN-K diagram indicates that the shale was not subjected to potassium metasomatism during diagenesis. Observed LREE enrichment, HREE depletion, negative Ce anomalies and positive Eu anomalies, all rule out seawater as the source of REEs and point toward felsic source rocks as the sediment source, which is supported by Al_2O_3/TiO_2 and TiO_2/Zr ratios. An LREE enrichment with negative Eu anomalies suggests that the Shanxi and Taiyuan Formations were more strongly affected by detrital input rather than by hydrothermal fluids.

Acknowledgements The research was supported by National Natural Science Foundation of China (Grant No. 41872178).

References

Algeo T J, Maynard J B (2004). Trace-element behavior and redox facies in core shales of Upper Pennsylvanian Kansas-type cyclothems. Chem Geol, 206(3–4): 289–318

Arthur M A, Sageman B B (1994). Marine black shales: depositional mechanisms and environments of ancient deposits. Annu Rev Earth Planet Sci, 22(1): 499–551

Bai F, Sun Y, Liu Y, Guo M (2017). Evaluation of the porous structure of Huadian oil shale during pyrolysis using multiple approaches. Fuel, 187: 1–8

Bai Y, Liu Z, Sun P, Liu R, Hu X, Zhao H, Xu Y (2015). Rare earth and major element geochemistry of Eocene fine-grained sediments in oil shale- and coal-bearing layers of the Meihe Basin, Northeast China. J Asian Earth Sci, 97: 89–101

Bezard R, Hébert R, Wang C, Dostal J, Dai J, Zhong H (2011). Petrology and geochemistry of the Xiugugabu ophiolitic massif, western Yarlung Zangbo suture zone, Tibet. Lithos, 125(1–2): 347–367

Birk D, White J C (1991). Rare earth elements in bituminous coals and underclays of the Sydney Basin, Nova Scotia: element sites, distribution, mineralogy. Int J Coal Geol, 19(1–4): 219–251

Chermak J A, Schreiber M E (2014). Mineralogy and trace element geochemistry of gas shales in the United States: environmental implications. Int J Coal Geol, 126: 32–44

Dai S, Li T, Seredin V V, Ward C R, Hower J C, Zhou Y, Zhang M, Song X, Song W, Zhao C (2014). Origin of minerals and elements in the Late Permian coals, tonsteins, and host rocks of the Xinde Mine, Xuanwei, eastern Yunnan, China. Int J Coal Geol, 121: 53–78

Dai S, Ren D, Chou C, Li S, Jiang Y (2006). Mineralogy and geochemistry of the No. 6 Coal (Pennsylvanian) in the Junger Coalfield, Ordos Basin, China. Int J Coal Geol, 66(4): 253–270

Dai S, Seredin V V, Ward C R, Hower J C, Xing Y, Zhang W, Song W, Wang P (2015b). Enrichment of U–Se–Mo–Re–V in coals preserved within marine carbonate successions: geochemical and mineralogical data from the Late Permian Guiding Coalfield, Guizhou, China. Miner Depos, 50(2): 159–186

Dai S, Yang J, Ward C R, Hower J C, Liu H, Garrison T M, French D, O'Keefe J M K (2015a). Geochemical and mineralogical evidence for a coal-hosted uranium deposit in the Yili Basin, Xinjiang, northwestern China. Ore Geol Rev, 70: 1–30

Douville E, Bienvenu P, Charlou J L, Donval J P, Fouquet Y, Appriou P, Gamo T (1999). Yttrium and rare earth elements in fluids from various deep-sea hydrothermal systems. Geochim Cosmochim Acta, 63(5): 627–643

Fu X, Wang J, Zeng Y, Tan F, He J (2011a). Geochemistry and origin of rare earth elements (REEs) in the Shengli River oil shale, northern Tibet, China. Chemistry, 71(1): 21–30

Fu X, Wang J, Zeng Y, Tan F, Feng X (2011b). Concentration and mode of occurrence of trace elements in marine oil shale from the Bilong Co area, northern Tibet, China. Int J Coal Geol, 85(1): 112–122

Gao P, Liu G, Jia C, Young A, Wang Z, Wang T, Zhang P, Wang D (2016). Redox variations and organic matter accumulation on the Yangtze carbonate platform during Late Ediacaran–Early Cambrian: constraints from petrology and geochemistry. Palaeogeogr Palaeocl Palaeoeco, 450: 91–110

Hakimi M H, Abdullah W H, Sia S G, Makeen Y M (2013). Organic geochemical and petrographic characteristics of Tertiary coals in the northwest Sarawak, Malaysia: implications for palaeoenvironmental conditions and hydrocarbon generation potential. Mar Pet Geol, 48: 31–46

Han S, Hu K, Cao J, Pan J, Xia F, Wu W (2015). Origin of early Cambrian black-shale-hosted barite deposits in South China: mineralogical and geochemical studies. J Asian Earth Sci, 106: 79–94

Han S, Zhang J, Wang C, Tang X (2018). Elemental geochemistry of lower Silurian Longmaxi shale in southeast Sichuan Basin, South China: constraints for paleoenvironment. Geol J, 53(4): 1458–1464

Hayashi K I, Fujisawa H, Holland H D, Ohmoto H (1997). Geochemistry of approximately 1.9 Ga sedimentary rocks from northeastern Labrador, Canada. Geochim Cosmochim Acta, 61(19): 4115–4137

He J, Ding W, Zhang J, Li A, Zhao W, Dai P (2016). Logging identification and characteristic analysis of marine–continental transitional organic-rich shale in the Carboniferous-Permian strata, Bohai Bay Basin. Mar Pet Geol, 70: 273–293

He T, Lu S, Li W, Sun D, Pan W, Zhang B, Tan Z, Ying J (2020). Paleoweathering, hydrothermal activity and organic matter enrichment during the formation of earliest Cambrian black strata in the northwest Tarim Basin, China. J Petrol Sci Eng, 189: 106987

He T, Lu S, Li W, Tan Z, Zhang X (2018). Effect of salinity on source rock formation and its control on the oil content in shales in the Hetaoyuan Formation from the Biyang Depression, Nanxiang Basin, Central China. Energ Fuels, 32(6): 6698–6707

Hofmann M H, Li X H, Chen J, MacKenzie L A, Hinman N W (2016). Provenance and temporal constraints of the Early Cambrian Maotianshan Shale, Yunnan Province, China. Gondwana Res, 37: 348–361

Hu J, Tang S, Zhang S (2016). Investigation of pore structure and fractal characteristics of the Lower Silurian Longmaxi shales in western Hunan and Hubei Provinces in China. J Nat Gas Sci Eng, 28: 522–535

Jones B, Manning D A (1994). Comparison of geochemical indices used for the interpretation of palaeoredox conditions in ancient mudstones. Chem Geol, 111(1–4): 111–129

Kasanzu C, Maboko M A H, Manya S (2008). Geochemistry of fine-grained clastic sedimentary rocks of the Neoproterozoic Ikorongo Group, NE Tanzania: implications for provenance and source rock weathering. Precambrian Res, 164(3–4): 201–213

Li Y, Tang D, Wu P, Niu X, Wang K, Qiao P, Wang Z (2016). Continuous unconventional natural gas accumulations of Carboniferous-Permian coal-bearing strata in the Linxing area, northeastern Ordos basin, China. J Nat Gas Sci Eng, 36: 314–327

Li Y, Fan T, Zhang J, Zhang J, Wei X, Hu X, Zeng W, Fu W (2015). Geochemical changes in the Early Cambrian interval of the Yangtze Platform, South China: implications for hydrothermal influences and paleocean redox conditions. J Asian Earth Sci, 109: 100–123

Li Y, Wang Z, Pan Z, Niu X, Yu Y, Meng S (2019a). Pore structure and its fractal dimensions of transitional shale: a cross section from east margin of the Ordos Basin, China. Fuel, 241: 417–431

Li Y, Wang Z, Gan Q, Niu X, Xu W (2019b). Paleoenvironmental conditions and organic matter accumulation in Upper Paleozoic organic-rich rocks in the east margin of the Ordos Basin, China. Fuel, 252: 172–187

Li Y, Wang Y, Wang J, Pan Z (2020a). Variation in permeability during CO_2–CH_4 displacement in coal seams: Part I—experimental insights. Fuel, 263: 116666

Li Y, Yang J, Pan Z, Tong W (2020b). Nanoscale pore structure and mechanical property analysis of coal: an insight combining AFM and SEM images. Fuel, 260: 116352

Ma L, Teng F Z, Jin L, Ke S, Yang W, Gu H O, Brantley S L (2015). Magnesium isotope fractionation during shale weathering in the Shale Hills Critical Zone Observatory: accumulation of light Mg isotopes in soils by clay mineral transformation. Chem Geol, 397: 37–50

McLennan S M (1993). Weathering and global denudation. J Geol, 101 (2): 295–303

McLennan S M (2001). Relationships between the trace element composition of sedimentary rocks and upper continental crust. Geochem Geophy Geosy, 2: 2000GC000109

Meng Q, Liu Z, Bruch A A, Liu R, Hu F (2012). Palaeoclimatic evolution during Eocene and its influence on oil shale mineralisation, Fushun basin, China. J Asian Earth Sci, 45: 95–105

Michard A, Albarède F (1986). The REE content of some hydrothermal fluids. Chem Geol, 55(1–2): 51–60

Murray R W (1994). Chemical criteria to identify the depositional environment of chert: general principles and applications. Sediment Geol, 90(3–4): 213–232

Nesbitt H, Young G (1982). Early Proterozoic climates and plate motions inferred from major element chemistry of lutites. Nature, 299(5885): 715–717

Nesbitt H, Young G (1984). Prediction of some weathering trends of plutonic and volcanic rocks based on thermodynamic and kinetic considerations. Geochim Cosmochim Acta, 48(7): 1523–1534

Newport L P, Aplin A C, Gluyas J G, Greenwell H C, Gröcke D R (2016). Geochemical and lithological controls on a potential shale reservoir: Carboniferous Holywell Shale, Wales. Mar Pet Geol, 71: 198–210

Olivarez A M, Owen R M (1991). The europium anomaly of seawater: implications for fluvial versus hydrothermal REE inputs to the oceans. Chem Geol, 92(4): 317–328

Qiu X, Liu C, Mao G, Deng Y, Wang F, Wang J (2014). Late Triassic tuff intervals in the Ordos Basin, Central China: their depositional, petrographic, geochemical characteristics and regional implications. J Asian Earth Sci, 80: 148–160

Qiu X, Liu C, Wang F, Deng Y, Mao G (2015). Trace and rare earth element geochemistry of the Upper Triassic mudstones in the southern Ordos Basin, Central China. Geol J, 50(4): 399–413

Sarki Yandoka B M, Abdullah W H, Abubakar M B, Hakimi M H, Adegoke A K (2015). Geochemistry of the Cretaceous coals from Lamja Formation, Yola Sub-basin, Northern Benue Trough, NE Nigeria: implications for paleoenvironment, paleoclimate and tectonic setting. J Afr Earth Sci, 104: 56–70

Stepanova V A, Pokrovsky O S, Viers J, Mironycheva-Tokareva N P, Kosykh N P, Vishnyakova E K (2015). Elemental composition of peat profiles in western Siberia: effect of the micro-landscape, latitude position and permafrost coverage. Appl Geochem, 53: 53–70

Sun Y, Zhao C, Qin S, Xiao L, Li Z, Lin M (2016). Occurrence of some valuable elements in the unique 'high-aluminium coals' from the Jungar coalfield, China. Ore Geol Rev, 72: 659–668

Tang L, Song Y, Jiang Z, Jiang S, Li Q (2019). Pore structure and fractal characteristics of distinct thermally mature shales. Energ Fuels, 33 (6): 5116–5128

Tao S, Shan Y, Tang D, Xu H, Li S, Cui Y (2016). Mineralogy, major and trace element geochemistry of Shichanggou oil shales, Jimusaer, Southern Junggar Basin, China: implications for provenance, palaeoenvironment and tectonic setting. J Petrol Sci Eng, 146: 432–445

Tribovillard N, Algeo T J, Lyons T, Riboulleau A (2006). Trace metals as paleoredox and paleoproductivity proxies: an update. Chem Geol, 232(1–2): 12–32

Udchachon M, Thassanapak H, Feng Q, Burrett C (2017). Palaeoenvironmental implications of geochemistry and radiolarians from Upper Devonian chert/shale sequences of the Truong Son fold belt, Laos. Geol J, 52(1): 154–173

Vosoughi Moradi A, Sarı A, Akkaya P (2016a). Geochemistry of the Miocene oil shale (Hançili Formation) in the Çankırı-Çorum Basin, Central Turkey: implications for Paleoclimate conditions, source–area weathering, provenance and tectonic setting. Sediment Geol, 341: 289–303

Vosoughi Moradi A, Sarı A, Akkaya P (2016b). Paleoredox reconstruction of bituminous shales from the Miocene Hançili Formation, Çankırı-Çorum Basin, Turkey: evaluating the role of anoxia in accumulation of organic-rich shales. Mar Pet Geol, 78: 136–150

Wang J, Chen D, Wang D A N, Yan D, Zhou X, Wang Q (2012). Petrology and geochemistry of chert on the marginal zone of Yangtze Platform, western Hunan, South China, during the Ediacaran-Cambrian transition. Sedimentology, 59(3): 809–829

Wang S, Dong D, Wang Y, Li X, Huang J, Guan Q (2016). Sedimentary geochemical proxies for paleoenvironment interpretation of organic-rich shale: a case study of the Lower Silurian Longmaxi Formation, Southern Sichuan Basin, China. J Nat Gas Sci Eng, 28: 691–699

Wang S, Zou C, Dong D, Wang Y, Li X, Huang J, Guan Q (2015). Multiple controls on the paleoenvironment of the Early Cambrian marine black shales in the Sichuan Basin, SW China: geochemical and organic carbon isotopic evidence. Mar Pet Geol, 66: 660–672

Xiao X M, Zhao B Q, Thu Z L, Song Z G, Wilkins R W T (2005). Upper

Paleozoic petroleum system, Ordos Basin, China. Mar Pet Geol, 22 (8): 945–963

Xiong F, Jiang Z, Huang H, Wen M, Moortgat J (2019). Mineralogy and gas content of Upper Paleozoic Shanxi and Benxi Shale Formations in the Ordos Basin. Energy Fuels, 33(2): 1061–1068

Xu G, Hannah J L, Bingen B, Georgiev S, Stein H J (2012). Digestion methods for trace element measurements in shales: paleoredox proxies examined. Chem Geol, 324-325: 132–147

Xu H, Tang D, Tang S, Zhang W, Meng Y, Gao L, Xie S, Zhao J (2015). Geologic and hydrological controls on coal reservoir water production in marine coal-bearing strata: a case study of the Carboniferous Taiyuan Formation in the Liulin area, eastern Ordos Basin, China. Mar Pet Geol, 59: 517–526

Yang C, Xiong Y, Zhang J, Liu Y, Chen C (2019). Comprehensive understanding of OM-hosted pores in transitional shale: a case study of Permian Longtan Shale in South China based on organic petrographic analysis, gas adsorption, and X-ray diffraction measurements. Energy Fuels, 33(9): 8055–8064

Yang H, Fu J, Wei X, Liu X (2008). Sulige field in the Ordos Basin: geological setting, field discovery and tight gas reservoirs. Mar Pet Geol, 25(4–5): 387–400

Yang N, Tang S, Zhang S, Chen Y (2015). Mineralogical and geochemical compositions of the No. 5 coal in chuancaogedan mine, Junger Coalfield, China. Minerals (Basel), 5(4): 788–800

Yang N, Tang S, Zhang S, Chen Y (2016). Modes of occurrence and abundance of trace elements in Pennsylvanian coals from the Pingshuo Mine, Ningwu Coalfield, Shanxi Province, China. Minerals (Basel), 6(2): 40

Zhang J, Fan T, Algeo T J, Li Y, Zhang J (2016). Paleo-marine environments of the Early Cambrian Yangtze Platform. Palaeogeogr Palaeocl Palaeoeco, 443: 66–79

Zhang S, Tang S, Tang D, Pan Z, Yang F (2010). The characteristics of coal reservoir pores and coal facies in Liulin district, Hedong coal field of China. Int J Coal Geol, 81(2): 117–127

Zhao J, Xu H, Tang D, Mathews J P, Li S, Tao S (2016a). Coal seam porosity and fracture heterogeneity of macrolithotypes in the Hancheng Block, eastern margin, Ordos Basin, China. Int J Coal Geol, 159: 18–29

Zhao J, Tang D, Xu H, Li Y, Li S, Tao S, Lin W, Liu Z (2016b). Characteristic of *in situ* stress and its control on the coalbed methane reservoir permeability in the eastern margin of the Ordos Basin, China. Rock Mech Rock Eng, 49(8): 3307–3322